Fusion Engineering and Design 202 (2024) 114380

Contents lists available at ScienceDirect

Fusion Engineering and Design

journal homepage: www.elsevier.com/locate/fusengdes

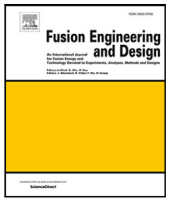

RELAP5/Mod3.3 MHD module development and validation: WCLL-TBM mock-up model

Lorenzo Melchiorri *, Simone Siriano, Alessandro Tassone

Nuclear Engineering Research Group, DIAEE - Sapienza University of Rome, Corso Vittorio Emanuele II 244, 00186 Rome, Italy

ARTICLE INFO

Keywords:
MHD
Pressure drop
Liquid metal
System magneto-thermal-hydraulic code
Breeding blanket

ABSTRACT

Magnetohydrodynamic (MHD) phenomena significantly impact the design of magnetic-confinement fusion reactors, particularly in the context of breeding blankets (BB) utilizing liquid metals (LMs) as working fluids. These effects arise from the interaction between the electro-conductive flowing metal and the magnetic field used for plasma confinement in the reactor chamber. Induced electrical currents in the liquid generate Lorentz forces, thereby altering flow behaviour in comparison to standard hydrodynamic conditions. For example, MHD effects modify velocity distribution and mass transport within ducts, amplify pressure losses, and influence heat transfer mechanisms. Accurate estimation of these impacts is crucial for the effective design of a liquid metal breeding blanket. While computational tools are essential for fusion-related physical analyses, no comprehensive MHD code currently exists for simulating all relevant phenomena in a liquid metal blanket. In this context, models predicting both distributed and concentrated MHD pressure drops have been integrated into the thermal-hydraulic system code RELAP5/Mod3.3. The Verification and Validation (V&V) process compares code results to direct numerical simulations and experimental data. For validation, RELAP5 recreates experimental results of a Water Cooled Lithium Lead test blanket module at magnetic field intensities ranging from $Ha = 500 - 3000$, confirming the reliability of the newly implemented MHD subroutines for predicting pressure drops within this parameter range.

1. Introduction

In nuclear fusion reactor engineering, liquid metals (LMs) are viewed as favourable working fluids, owing to their advantageous properties both as coolants and as tritium breeders or carriers. Due to their high electrical conductivity, LMs experience self-induced Lorentz forces when they flow in strong magnetic fields, leading to the emergence of magnetohydrodynamic (MHD) effects. These effects alter flow rate distribution, increase pressure drops, and impact turbulent flow and heat transfer mechanisms, thereby affecting the performance of breeding blankets [1–3]. For accurate and reliable breeding blanket (BB) design, it is crucial to develop numerical codes capable of predicting these MHD phenomena.

Generally, blanket-scale MHD analyses employ a semi-analytical approach, integrating empirical and semi-empirical correlations with data from direct numerical simulations [4–6]. However, this approach is computationally expensive and lacks flexibility. While some computational fluid dynamics (CFD) software has dedicated MHD modules [3], these are not employable for reactor-scale simulations due to computational resource limitations. System thermal-hydraulic (STH) codes offer efficient reactor-level simulations but currently lack comprehensive MHD capabilities, as highlighted in Ref. [7].

The Nuclear Energy Research Group (NERG) at Sapienza University of Rome is developing a modified version of RELAP5/Mod3.3 to incorporate MHD pressure drop calculations for complex geometries. The development is termed RELAP5 Development for Magnetohydraulics or REDMaHD. Details of the implemented models and a preliminary Verification and Validation (V&V) procedure have been extensively discussed in previous works presented in [8]. Even in its current state, REDMaHD shows competitive capabilities in modelling MHD phenomena compared to existing STH codes, as reviewed in Refs. [9, 10].

This study aims to progress the validation process of the code another step forward. Courtessole et al. led an experimental campaign on a scaled-down version of the Water-Cooled Lithium Lead (WCLL) Test Blanket Module (TBM), with the key findings discussed in [11,12]. The data sheds light on the MHD pressure drops within the module and how the LM mass flow rate is distributed among the eight breeding units (BUs). To capture the details, the mock-up hydraulic circuit has been simulated using REDMaHD, aiming for a high level of fidelity to

* Corresponding author.
E-mail address: lorenzo.melchiorri@uniroma1.it (L. Melchiorri).

https://doi.org/10.1016/j.fusengdes.2024.114380
Received 13 October 2023; Received in revised form 28 February 2024; Accepted 19 March 2024

each geometric feature. Several calculations were then performed, to simulate closely the experimental tests. When comparing the results from the code to the experimental data, it becomes clear that the numerical tool is quite adept at reproducing the underlying physics, especially when the magnetic field strength is closer to the one expected in a fusion reactor Ha $\approx 10^4$.

2. MHD basic theory

In the presence of a magnetic field, internal electrical currents are induced in the body of a flowing electrically conductive fluid. These currents consequently interact with the external magnetic field to give rise to Lorentz forces that tend to counteract fluid motion. To adequately describe these interactions, the governing equations for MHD are formulated by combining the Navier–Stokes and Maxwell equations. Specifically, for MHD LM flows relevant to fusion reactors, one can employ the assumption of negligible magnetic Reynolds number, the so called "inductionless" approximation. This assumption effectively removes the fluid feedback on the imposed magnetic field through the self-induced one, thereby simplifying the otherwise non-linear coupling existing between the fluid velocity and magnetic field [1]. For the scope of this research, emphasis is placed on the non-dimensional form of the momentum balance equation, where the Lorentz force is introduced as a source term on the right-hand side of the equation:

$$\frac{1}{\mathrm{N}}\left[\frac{\partial \mathbf{v}}{\partial t}+(\mathbf{v}\cdot\nabla)\mathbf{v}\right]=-\nabla p+\frac{1}{\mathrm{Ha}^2}\nabla^2\mathbf{v}+\mathbf{j}\times\mathbf{B} \tag{1}$$

In Eq. (1), the vectors **v**, **j**, and **B** represent the velocity, current density, and magnetic field, respectively, while p denotes pressure. Dimensionless quantities are obtained by scaling with the reference velocity v_0, $j_0 = \sigma v_0 B_0$, the characteristic length a and the external magnetic field strength B_0. The parameter a depends on the specific case under consideration, but is usually taken as the half-length of a duct in the direction of the magnetic field. The dimensionless pressure p is generally scaled via $p_0 = \sigma v_0 a B_0^2$.

Two essential parameters govern the flow: the Hartmann number $\mathrm{Ha} = aB_0\sqrt{\sigma/\mu}$ and the Stuart number, also known as the interaction parameter $\mathrm{N} = \sigma a B_0^2/\rho v_0$. The square of Ha characterizes the relative influence of electromagnetic to viscous forces, while N indicates the ratio of electromagnetic to inertial forces. Symbols σ, μ, and ρ represent the fluid electrical conductivity, dynamic viscosity, and density, respectively. Ha and N can also be rearranged to yield the classical Reynolds number as $\mathrm{Re} = \mathrm{Ha}^2/\mathrm{N} = \rho v_0 a/\mu$.

In fusion blanket applications, both Ha and N typically attain high values ($\approx 10^4$), justifying the statement that electromagnetic forces dominate the flow features compared with viscous and inertial effects in most MHD flows. One of the most important MHD flow features is the development of so-called "core" region where, if Ha $\gg 1$ the force balance is restricted to Lorenz and pressure forces, while viscous effects remain relevant in thin fluid layers near solid walls, known as Hartmann and side layers. These may appear, for the simple case of a rectangular duct, depending on the wall orientation with regard to the imposed field (perpendicular and parallel).

Another crucial non-dimensional parameter is the wall conductance ratio $c = \sigma_w t_w/\sigma a$, representing the tendency of induced currents to complete their circuits through the fluid or adjacent walls. The value of c is very influential on the flow characteristics. In general, a higher conductance ratio correlates with increased additional MHD pressure losses. The velocity profile in a channel cross-section can also vary depending on c, possibly leading to fluid overshoots near conductive walls. Additionally, the conductance ratio serves as a key parameter for characterizing phenomena such as the Madarame effect or electromagnetic coupling [13]. This effect occurs when different channels share walls and can interact by exchanging electric currents across these walls. The MHD pressure drops are generally addressed

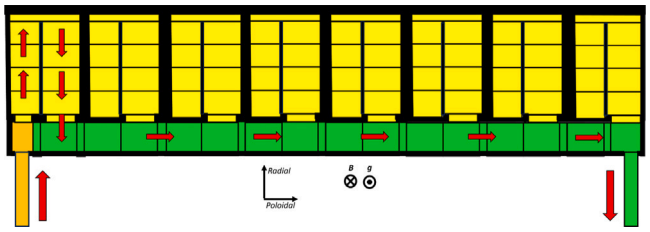

Fig. 1. Radial–poloidal sketched view of the mock up. Red arrows serve to highlight one of the possible hydraulic path, specifically the one through the first breeding unit (BU1). B is the magnetic field vector and g the gravitational acceleration.

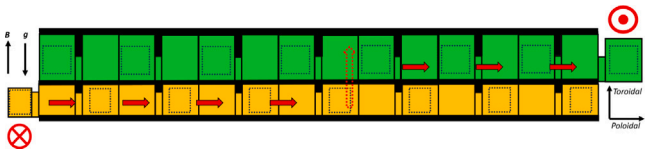

Fig. 2. Radial–poloidal sketched view of the mock up. Red arrows serve to highlight one of the possible hydraulic path, specifically the one through the fifth breeding unit (BU5). B is the magnetic field vector and g the gravitational acceleration.

using a hydrodynamic-like approach, where the overall loss $\Delta P_{\mathrm{MHD}} = \Delta P_{2D} + \Delta P_{3D}$ [14]. The two-dimensional MHD pressure drop ΔP_{2D} is analogous to ordinary friction (or distributed) losses, caused by Lorenz forces that arise from currents closing their paths perpendicularly to the flow direction. Unlike ΔP_{2D}, the three-dimensional MHD pressure drops ΔP_{3D} are more challenging to quantify. Those may be compared to the hydraulic local (or concentrated) losses, they can be caused by complex geometric features and non-uniform electromagnetic boundary conditions, which are often encountered in fusion reactors. They generally occur when the fluid is forced to deviate from its fully developed conditions, such as due to the presence of bends or abrupt changes in the channel area. The resulting currents are then allowed to close also along the direction of the fluid flow [15–17].

3. Reference geometry and numerical model

All the relevant information and a detailed description of how the experiments have been performed can be found in Refs. [11,18]; an abridged version is provided thereafter. A scaled 1 : 2.5 mock-up of the WCLL TBM, capturing all essential geometric features, was developed for MHD experiments in MEKKA laboratory. Designed for horizontal orientation within the lab magnet gap, the mock-up has dimensions of 668.4×222.6×102 mm^3, fitting well into the homogeneous magnetic field area. Particular attention was given to accurately replicating manifold geometries, as they contribute the most to pressure drop. Fabricated from 1.4571 austenitic steel, the mock-up minimizes magnetic field distortions and is compatible with the sodium-potassium (NaK) liquid alloy employed as dummy fluid instead of the lead-lithium foreseen in the actual blanket.

Figs. 1 and 2 showcase the schematic representations of the mock-up as simulated in the system code. The area highlighted in orange encompasses the inlet pipe and the feeder (or inlet manifold). The yellow region represents the breeding zone, which is divided into eight separate breeding units (BU). The green portion illustrates the collector (also known as draining manifold) and the outlet pipe. The mock-up lays horizontally (labelled as the radial–poloidal plane in Fig. 1, in analogy with the ITER coordinate system for the actual WCLL TBM) in the magnet gap and, thus, the magnetic field is supposed to have only the vertical component as non-zero (the toroidal component, following the same analogy). Fig. 2 illustrates how the feeder and collector lays side by side in the magnetic field direction.

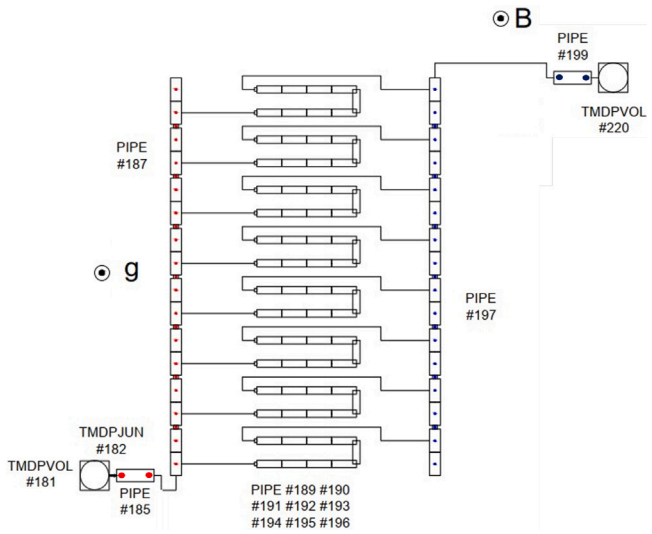

Fig. 3. RELAP5 nodalization scheme of the circuit. The names of the components (number) are arbitrary and do not have any impact on the calculations. Red and blue dots represent the points where the code samples the data shown in Section 4.

Concerning the actual nodalization scheme employed, this is presented in Fig. 3. The thermodynamic conditions of the LM at the inlet and outlet (i.e., temperature and pressure) are set using two time-dependent volumes (TMDPVOL #181 and #220). A time-dependent junction (#182) enforces the assumed mass flow rate throughout the circuit. Pipe component #185 simulates the radial inlet channel. Each manifold is modelled using a pipe component consisting of 23 control volumes (CVs), which mimics the chambers constituting the manifolds and their interconnections. Lateral junctions couple the BUs to the corresponding volumes in the distributing and draining manifold. Every BU is replicated using a pipe component that comprises 11 CVs: 8 for the radial length, 1 for the curve and 2 for the inlet/outlet windows. The outlet manifold (#197) employs the same slice modelling approach used for the inlet manifold (#187), reflecting the actual geometric characteristics. The LM exiting the mock-up is collected in the outlet pipe (#199) and drains into TMDPVOL #220.

It is worth mentioning that the two junctions connecting #185 with #187 and #197 with #199 do not precisely replicate the geometry of the mock-up. Specifically, the poloidal–toroidal cross-sectional area of the first CV in the distributing manifold and the last CV in the draining manifold has been halved [11,18]. This effectively means that each of these control volumes is half the size it should be. This adjustment was made because the missing halves would have constituted isolated volumes or "dead branches", according to the nodalization criteria of RELAP5, meaning they would have been regions of stagnant flow. Given that REDMaHD is not currently configured to accurately model such elements, a more simplified nodalization approach was adopted.

Using the grid configuration described, the simulations referenced in Section 4 have run times ranging from 20 seconds to 2 minutes on a single i7-11700K CPU.

The study is carried out under isothermal conditions with a reference temperature of $T_{\mathrm{Ref}} = 300\,\mathrm{K}$ and a reference pressure of $p_{\mathrm{Ref}} = 0.1\,\mathrm{MPa}$. The thermophysical properties of the materials involved are computed at these conditions and are listed in Table 1. Correlations for the NaK properties are taken from Ref. [19], while properties for steel are taken from [11].

All computations are led under conditions of steady-state. In total, thirteen different scenarios were simulated, each varying in magnetic field strength and mass flow rate. The parameters range for these simulations is $500 \leq \mathrm{Ha} \leq 3000$ and $200 \leq \mathrm{Re} \leq 2000$. These values are calculated based on representative scales for the BU, hence the

Table 1
Material properties at $T_{\mathrm{Ref}} = 300\,\mathrm{K}$ and $p_{\mathrm{Ref}} = 0.1\,\mathrm{MPa}$.

Material	σ [S/m]	ρ [kg/m^3]	μ [Pa s]
NaK	2.61×10^6	872.3	8.1×10^{-4}
Stainless steel	1.25×10^6	–	–

characteristic velocity $v_0 = \frac{\Gamma}{8\rho(A_{\mathrm{BU}}/2)}$, which depends on the Γ of the test considered, and the characteristic length $a_{\mathrm{BU}} = 0.039\,[\mathrm{m}]$, chosen as half of the internal toroidal dimension of a single BU. Here, $\Gamma[\frac{\mathrm{kg}}{\mathrm{s}}]$ denotes the total mass flow rate across the eight breeding units, each with a cross-sectional area $A_{\mathrm{BU}} = 5.8 \cdot 10^{-3}\,[\mathrm{m}^2]$.

Pressure scaling utilizes different characteristic quantities in order to be consistent with the approach described in Refs. [11,12] where these are defined considering the flow state in the manifold since the pressure losses in those components are the most significant factors for pressure distribution in the mock-up. Because the cross-sectional areas of these manifolds are smaller than those of the BUs, its characteristic velocity, defined as $v_{\mathrm{man}} = \Gamma/\rho A_{\mathrm{man}}$, is going to be different. In this equation, $A_{\mathrm{man}} = 1.87 \cdot 10^{-3}\,[\mathrm{m}^2]$ is the average cross-sectional area of the feeding and draining channels of the manifold. Additionally, the manifold channel half-width in the magnetic field direction, $a_{\mathrm{man}} = 0.0195\,[\mathrm{m}]$, is reduced compared to a_{BU}. Therefore, the metric for assessing pressure distribution involves a scaled pressure variable p/p_{man}, defined as $p_{\mathrm{man}} = \sigma v_{\mathrm{man}} a_{\mathrm{man}} B^2$.

It should be noted that in a complex geometry like that of the MEKKA mock-up, electromagnetic coupling is expected to affect the LM flow. In the manifold region, the distributing and draining channels are separated by a common wall, referred to as the baffle plate. In this region, the LM flows in the same direction on both side of the partition resulting, in general, in a favourable impact on pressure drop due to a mutually beneficial "pumping" effect when the mass flow rate in the two channels is equal [20,21]. In the REDMaHD model the thickness of the Hartmann walls, the upper one for the distributing channel and the lower one for the draining channel, is considered to be half of the actual thickness of the shared plate. This adjustment is a methodological consideration to partially emulate the electromagnetic coupling effects, enhancing the model representation of altered current distribution and resistance in the baffle plate that yields to a reduced pressure loss [20,22].

It should be remarked that the condition of equal mass flow rate in the two manifold channels is not usually fulfilled but, rather, the imbalance tends to grow the further away the considered section is compared with the equatorial section of the mock-up (BU4/5). Focusing on the manifold terminal sections, CFD analyses have highlighted that this condition is responsible for a pressure build-up in the channel with the smaller flow rate and the onset of a peculiar flow regime [23]. The effect of this phenomenon on the overall pressure drop seems to be minimal, though, as demonstrated by Ref. [10], in which we were able to recreate with good accuracy the pressure drop distribution in the same configuration used in Ref. [23] with REDMaHD.

Conversely, for the walls shared by the BUs, the NaK flow is in counter-flow, leading to an increased pressure drop compared to a stand-alone duct [24]. Consequently, the entire poloidal thickness of the mock-up plates is considered in our model to represent the BU side walls. It should be noted that, in principle, the Madarame effect should also be present between the BUs and the manifolds, which share 3D currents generated at their interface (simultaneous cross-section variation and change of stream direction perpendicular to the magnetic field plane). It is not yet clear the importance of this effect on the system pressure drop but its simulation currently exceeds the capabilities of the REDMaHD model.

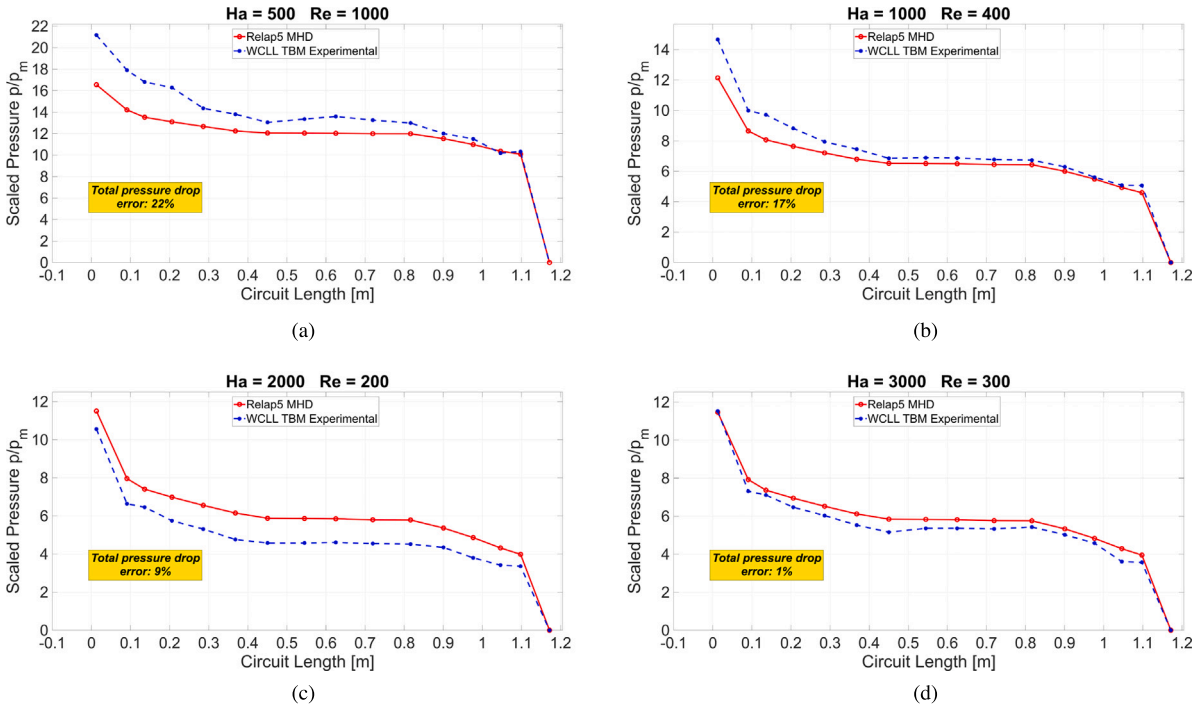

Fig. 4. Comparison between REDMaHD and experimental tests, in terms of scaled pressure drops along the circuit length of the mockup as defined in [11].

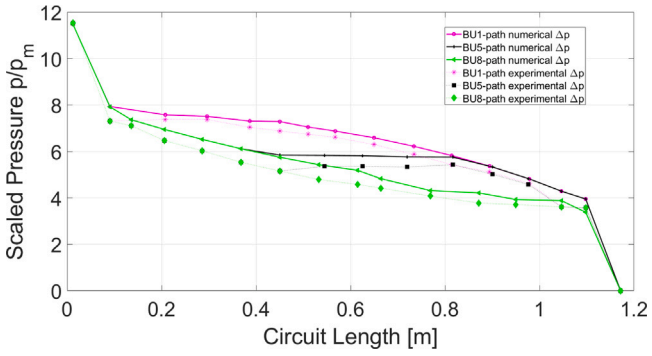

Fig. 5. Scaled pressure versus circuit length for Ha = 3000 and Re = 300, REDMaHD outcomes are compared with experimental data. Three different flow paths are highlighted for the first,middle and last breeding unit.

Table 2
Discrepancy (%) between REDMaHD outcomes and various experimental tests, in terms of total pressure drop within the mockup.

Hartmann	Reynolds	Pressure drop error (%)
500	1000	22
500	2000	22
500	3000	23
1000	400	17
1000	600	16
1000	800	16
1000	1000	18
1000	2000	19
2000	200	9
2000	400	2
2000	600	3
2000	800	2
3000	300	1

4. Results and discussion

In Fig. 4, the REDMaHD outcomes are compared with various experimental data. The results are reported in terms of scaled pressure drops, as delineated in Section 3. For the sake of clarity, the diagrams refer to the hydraulic path through the fifth BU, which nonetheless serves to emphasize key features of the LM flow. The associated relative errors for the total loss of load are summarized in Table 2.

The majority of the total pressure drop Δp_{tot} occurs in the inlet and outlet circular pipes as well as in the manifolds. In the BUs, the pressure drop is relatively small. However, there exists a discrepancy in the pressure drops between BU1 and BU8 in contrast to the other BUs, attributable to the notable differences in mass flow rate distribution among the units, as discussed subsequently.

It should be noted that contrary to what was described in [8], the ΔP_{2D} model adopted in this study has been refined using the Tillack formulation for the fully developed MHD pressure gradient [25]. This formulation is deemed more representative as it accounts for the effects of viscosity at large but finite Ha, albeit with a marginal impact on the total pressure loss in the mockup. The loss is found to be on average $\approx 2\%$ more precise than the earlier correlation for this particular range of Hartmann numbers. The ΔP_{3D} model remains unaltered relative to the one presented in [8]. The purely hydraulic distributed pressure losses in the mockup module amount to approximately $0.5 - 1\%$ of the total. For hydrodynamic localized drops, the k factor has been specified during the geometry modelling phase, following guidelines provided in the Idel'chik handbook for complex geometries such as bends or abrupt area changes [26,27].

From Figs. 4, 5, and the data gathered in Table 2, it becomes evident that the results produced by REDMaHD are in a reasonable agreement with the experimental data. This agreement improves notably when both the Hartmann number (Ha) and interaction parameter (N) are increased. Such behaviour aligns well with expectations, as the correlations implemented within the code are particularly formulated to address fluid flows that are relevant to fusion conditions, where MHD effects are dominant over inertial and viscous forces. When the interaction parameter N is decreased, the model tends to deviate more from the experimental data, although this deviation remains within an acceptable range. The primary source of this deviation can be attributed to the pressure losses that occur in

Table 3
Percentage relative errors of the pressure gradient calculated by REDMaHD and the experimental data. The pressure gradient is calculated as the pressure difference between two consecutive taps dived for the distance.
Source: The identifying name of the pressure taps are taken from [11].

Hartmann	2000	2000	2000	2000	3000	Regions
Reynolds	200	400	600	800	300	
Taps name	Relative errors (%) on the pressure gradient					
H5-L1	9.61	14.43	17.80	15.10	16.06	Region 1 Inlet
L1 - H2	210.17	116.61	109.00	77.30	178.22	
H2-L5	41.05	43.98	44.90	42.60	34.83	Inlet manifold
L5-H3	2.33	1.93	13.90	25.70	2.59	
H3-L10	26.53	21.92	23.60	18.90	19.35	
L10-H4	52.39	5.56	1.00	9.30	25.83	
H4-L16	−14.53	18.16	9.25	−28.15	−26.96	BU5
L16-L19	149.16	77.44	57.50	42.00	3.19	Outlet manifold
L19-L22	8.54	8.02	2.80	5.50	14.15	
L22-L23	42.55	18.56	7.60	5.60	44.24	
L23-L20	462.55	463.66	1583.10	3261.50	744.60	Region 2 outlet
L20-L21	18.59	15.27	8.30	8.20	10.70	

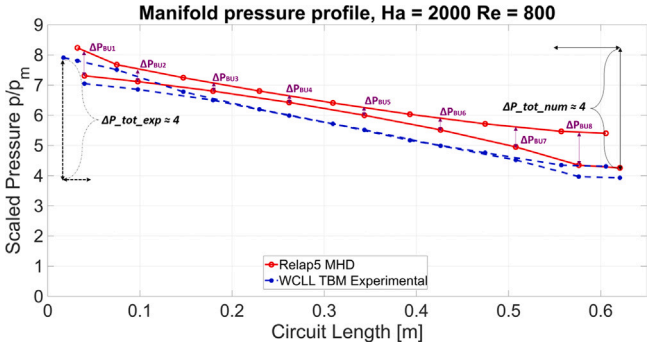

Fig. 6. Details of the non-dimensional pressure drop in the manifold regions are presented. The upper curve for each colour represents the pressure loss in the distributing manifold, while the lower curve corresponds to the draining manifold. The pressure head for each unit is indicated in purple.

the manifold regions right after the inlet pipe and just before the outlet channel. Those regions are characterized by the simultaneous presence of abrupt changes in cross-sectional area and bends. Even at high values of the magnetic field, characterizing the phenomena occurring in those parts of the test section rigorously through the code remains challenging.

In Table 3 are collected the data concerning the relative errors between computed and measured pressure gradients among consecutive taps. The positions of these taps are indicated by the markers in Figs. 4 and 5. Notably, the highest error is observed in both the entrance and exit regions, denoted as Region 1 and Region 2, which encompass the first three and the last three pressure measurement points, respectively.

A deeper understanding of the observed behaviour can be gained by considering that in those specific areas the governing parameters, and thus the interactions between forces of various types, deviate from the reference values for the breeding zone, as specified in Section 3. For instance, in a case marked by Ha = 2000 and Re = 800, the governing parameters in the entrance region can be approximated as Ha ≈ 200 and Re ≈ 16000, with an interaction parameter of N ≈ 2.5. These estimates are based on the characteristic length of the circular inlet/outlet pipe ($a_{circ} = 8 \cdot 10^{-3}$ m) and an average NaK velocity ($v \approx 2.24$ m/s).

Therefore, REDMaHD functions under MHD and geometrical conditions that differ considerably from its intended application. The code $\Delta P_{exp-contr}$ MHD model, that is likely to contribute the most in that part of the grid, is calibrated for high interaction parameters ($N \gg 10$) and scenarios where fully developed flow conditions are established upward/downward the sudden variation [8]. The complex geometry in Region1 and Region2 introduces inertial phenomena not currently accounted for in the model. For example in Region1, which interfaces with the distributing manifold and the first breeding unit, differs significantly from a long straight duct. The inlet pipe and the BU1 inlet window are facing each other, causing most of the flow to be directed through the latter. The cross-sectional area of this window is approximately 33% smaller than that of the distributing manifold, contributing to considerable pressure loss in that part of the mock-up. However, this specific pressure loss becomes less significant as the magnetic field strengthens and the flow is increasingly governed by MHD forces.

The local pressure drop coefficient $k_{MHD-exp/contr}$ is formulated under the assumption that symmetrical expanding and contracting geometries result in equivalent pressure losses [8]. This assumption holds reasonably well only for flows characterized by high Ha and N [28]. This is corroborated by the experimental data presented in Fig. 4. Pressure losses in the exit region, which connects BU8 to the draining manifold and subsequently to the outlet channel, vary considerably from those in the inlet region at lower Ha values. As the magnetic field increases, these losses begin to exhibit a more symmetrical behaviour. Fig. 4(a) [29].

In Fig. 6, the predicted pressure losses within the manifold region are presented. Given that these losses constitute the dominant contribution to the overall pressure drop in the experiment, they can serve as a reliable test for the model accuracy. The pressure losses calculated using REDMaHD closely resemble those obtained from experimental data. However, the red and blue curves begin and end at different ordinate values, which is likely a result of the different pressure losses calculated by the code in the regions immediately following or preceding the inlet and outlet channels. On the other end, the gap between the pressure profiles in the two manifolds essentially represents the pressure head available for each BU and serves as a direct measure of the mass flow rate passing through it. For this metric, we observe a significant deviation from the experimental data.

In Fig. 7, the mass flow rate distribution among the BUs is displayed, normalized to $\Gamma/8$. The experiments indicate that the bulk of the mass flow rate is actually circulated through BU1 and BU8, a feature that is adequately captured by REDMaHD in a qualitative sense, but not in a quantitative one. This discrepancy may be due to the unique layout, as already discussed, in which the inlet channel directly faces BU1, causing the fluid to exit the inlet pipe at a high velocity. As a result, the fluid inertia conveys it preferentially into BU1. Even at high magnetic field strengths, this behaviour is not adequately dampened. The model starts to yield a more accurate depiction of the mass flow rate distribution only when the magnetic field approaches its higher experimental value, as shown in Fig. 7(b). The deviation still observed in this more favourable case could be attributed to electromagnetic coupling phenomena occurring between the BUs, which are currently only coarsely accounted for in REDMaHD.

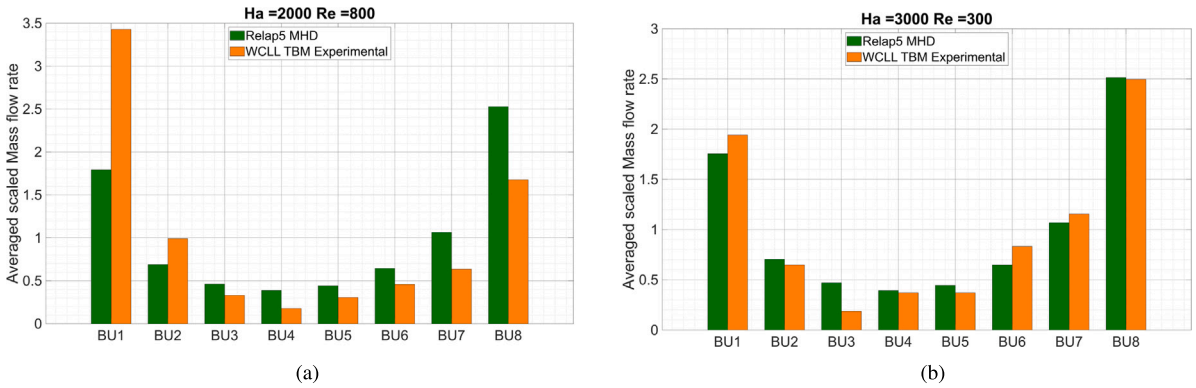

Fig. 7. Comparison of the distribution of the NaK mass flow rate among the breeding units: REDMaHD vs experimental data.

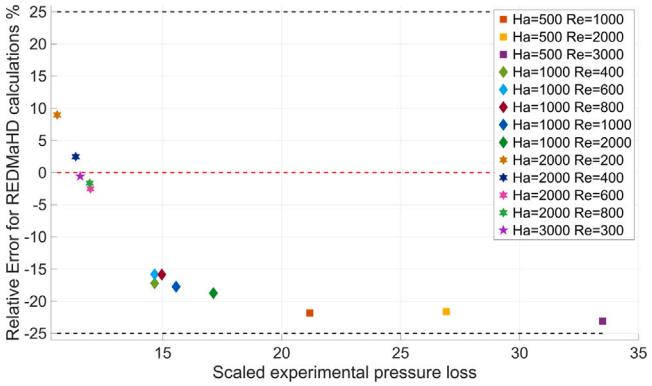

Fig. 8. Trend of the relative error in calculations towards the scaled pressure losses, for all the simulations performed.

5. Conclusions

This validation exercise has been intended to assess the capacity of REDMaHD to properly represent the MHD flow in a component of complex geometry such as the WCLL TBM mock-up. The research builds on experimental studies carried out at the MEKKA laboratory at KIT, which have been focused on the evaluation of pressure drops and flow partitioning in the manifolds and breeder units of a scaled WCLL TBM mock-up [11,12]. It can also be seen as a further substantiation of a previous activity performed on the actual WCLL TBM configuration [10] and a prosecution of the validation activities carried on in the past using numerical and experimental data [8].

The experimental data obtained at KIT have played a crucial role in the validation of the MHD module within the RELAP5/Mod3.3 code, known as REDMaHD, currently under development at Sapienza University of Rome. Initial results from RED-MaHD are encouraging, particularly in terms of accurately predicting the total pressure losses in high magnetic field environments. The outcomes of the validation benchmark are summarized in Fig. 8. In particular, they confirm the possibility to obtain a good prediction of the overall pressure loss, already ascertained in Ref. [8] for two different TBM configurations (the european Helium-Cooled Lead Lithium and the indian Lead Lithium Ceramic Breeder), while also recreating to an acceptable degree the local pressure profile.

Nonetheless, the study also highlights challenges related to achieving an accurate prediction of the mass flow rate distribution across the BUs, largely due to the limitations of REDMaHD in accurately capturing local inertia-driven phenomena and, possibly, large-scale electromagnetic coupling effects. Nevertheless, the STH code prediction is judged satisfactory even for this metric, since we have demonstrated that the accuracy of REDMaHD increases with the magnetic field intensity. In a sense, these results may increase the value of the study presented in Ref. [10], where REDMaHD was used for the optimization of the WCLL TBM geometry, since it provides an indication about the uncertainty on flow rate distribution.

Future work will concentrate on improve the predictive capabilities of REDMaHD by enhancing the ΔP_{3D} model to make it applicable to a wider range of geometrical conditions (gradual expansion, dependence on wall conductivity, etc.) and local governing parameters (better model of inertial effects). Additionally, a preliminary model to address electromagnetic coupling phenomena is in the conceptualization stage, along with a module designed to characterize forced convection heat transfer for perfectly insulated walls; a condition relevant for Dual Coolant BB.

CRediT authorship contribution statement

Lorenzo Melchiorri: Conceptualization, Investigation, Methodology, Visualization, Writing – original draft. **Simone Siriano:** Software, Writing – review & editing. **Alessandro Tassone:** Investigation, Visualization, Writing – review & editing.

Declaration of competing interest

The authors declare that they have no known competing financial interests or personal relationships that could have appeared to influence the work reported in this paper.

Data availability

The authors do not have permission to share data.

Declaration of Generative AI and AI-assisted technologies in the writing process

During the preparation of this work, the author(s) used the OpenAI GPT-4 language model, commonly known as ChatGPT, in order to improve the clarity and structure of English writing, as well as to assist with formatting tasks. After using this tool/service, the author(s) reviewed and edited the content as needed and take(s) full responsibility for the content of the publication.

Acknowledgements

This work has been carried out within the framework of the EUROfusion Consortium, funded by the European Union via the Euratom Research and Training Programme (Grant Agreement No 101052200 — EUROfusion). Views and opinions expressed are however those of the author(s) only and do not necessarily reflect those of the European Union or the European Commission. Neither the European Union nor the European Commission can be held responsible for them.

References

[1] U. Müller, L. Bühler, Magnetofluiddynamics in channels and containers, Springer-Verlag Berlin Heidelberg GmbH, Karlsruhe, 2001, [Online]. Available: http://download.springer.com/static/pdf/185/bfm{%}253A978-3-642-56668-4{%}252F1.pdf?auth66=1401995374{_}4d363c462609ae19e3de18b0ee51ef07{&}ext=.pdf.

[2] I.R. Kirillov, C.B. Reed, L. Barleon, K. Miyazaki, Present understanding of MHD and heat transfer phenomena for liquid metal blankets, Fusion Eng. Des. 27 (C) (1995) 553–569.

[3] S. Smolentsev, S. Badia, R. Bhattacharyay, L. Bühler, L. Chen, Q. Huang, H.G. Jin, D. Krasnov, D.W. Lee, E.M. De Les Valls, C. Mistrangelo, R. Munipalli, M.J. Ni, D. Pashkevich, A. Patel, G. Pulugundla, P. Satyamurthy, A. Snegirev, V. Sviridov, P. Swain, T. Zhou, O. Zikanov, An approach to verification and validation of MHD codes for fusion applications, Fusion Eng. Des. 100 (2015) 65–72.

[4] A. Tassone, S. Siriano, G. Caruso, M. Utili, A. Del Nevo, MHD pressure drop estimate for the WCLL in-magnet PbLi loop, Fusion Eng. Des. 160 (September 2019) (2020) 111830, http://dx.doi.org/10.1016/j.fusengdes.2020.111830.

[5] A. Tassone, G. Caruso, A. Del Nevo, Influence of PbLi hydraulic path and integration layout on MHD pressure losses, Fusion Eng. Des. 155 (July 2019) (2020) 111517, http://dx.doi.org/10.1016/j.fusengdes.2020.111517.

[6] J. Reimann, G. Benamati, R. Moreau, Report of working group MHD for the blanket concept selection exercise (BSE), no. FZKA 5652, 1995.

[7] S.B. Seo, R. Hernandez, M. O'Neal, N. Meehan, F.S. Novais, M. Rizk, G.I. Maldonado, N.R. Brown, A review of thermal hydraulics systems analysis for breeding blanket design and future needs for fusion engineering demonstration facility design and licensing, Fusion Eng. Des. 172 (2021) 112769.

[8] L. Melchiorri, V. Narcisi, F. Giannetti, G. Caruso, A. Tassone, Development of a RELAP5/MOD3. 3 module for MHD pressure drop analysis in liquid metals loops: Verification and Validation, Energies 14 (17) (2021) 5538.

[9] C. Mistrangelo, L. Bühler, C. Alberghi, S. Bassini, L. Candido, C. Courtessole, A. Tassone, F.R. Urgorri, O. Zikanov, MHD R&D activities for liquid metal blankets, Energies 14 (20) (2021) 6640, http://dx.doi.org/10.3390/en14206640.

[10] L. Melchiorri, V. Narcisi, C. Ciurluini, F. Giannetti, G. Caruso, A. Tassone, Preliminary MHD pressure drop analysis for the prototypical WCLL TBM with RELAP5/MOD3. 3, Fusion Eng. Des. 176 (2022) 113048.

[11] L. Bühler, C. Courtessole, C. Koehly, C. Mistangelo, Experimental Analysis of Magnetohydrodynamic Flows in a Scaled Mock-up of a WCLL Test Blanket Module, MEKKA - Report 2022 BB.TBM.S.02.01.T001-D004, Nuclear Fusion Programme, 2023, Report code: EFDA-D-2QHN97.

[12] C. Courtessole, H.-J. Brinkmann, J. Roth, L. Bühler, Experimental investigation of MHD flows in WCLL TBM mockup, 2023, Poster presentation at the 15th International Symposium on Fusion Nuclear Technology (ISFNT 2023), Las Palmas de Gran Canaria, Spain.

[13] H. Madarame, K. Taghavi, M.S. Tillack, Influence of leakage currents on MHD pressure drop, Fusion Technol. 8 (1 pt 2(A)) (1985) 264–269.

[14] S. Smolentsev, R. Moreau, L. Bühler, C. Mistrangelo, MHD thermofluid issues of liquid-metal blankets: Phenomena and advances, Fusion Eng. Des. 85 (7–9) (2010) 1196–1205, http://dx.doi.org/10.1016/j.fusengdes.2010.02.038.

[15] L. Bühler, S. Horanyi, Experimental investigations of MHD flows in a sudden expansion, Wiss. Berichte FZKA 7245 (August) (2006) 1–65, [Online]. Available: http://cat.inist.fr/?aModele=afficheN{&}cpsidt=18097940.

[16] T.J. Rhodes, S. Smolentsev, M. Abdou, Magnetohydrodynamic pressure drop and flow balancing of liquid metal flow in a prototypic fusion blanket manifold, Phys. Fluids 30 (5) (2018).

[17] L. Bühler, C. Mistrangelo, H.J. Brinkmann, Experimental investigation of liquid metal MHD flow entering a flow channel insert, Fusion Eng. Des. 154 (September 2019) (2020) 111484, http://dx.doi.org/10.1016/j.fusengdes.2020.111484.

[18] C. Koehly, L. Bühler, C. Courtessole, Design of a scaled mockup of the WCLL TBM for MHD experiments in liquid metal manifolds and breeder units, Fusion Eng. Des. 192 (2023) 113753.

[19] O. Foust, in: O. Foust (Ed.), Sodium-NaK Engineering Handbook, vol. I, Gordon and Breach, New York, 1972.

[20] X. Zhang, L. Wang, C. Pan, Effects of inclined transversal magnetic fields on magnetohydrodynamic coupling duct flow states in liquid metal blankets: Under uniform magnetic fields, Nucl. Fusion 61 (1) (2020) 016005.

[21] S. Siriano, A. Tassone, G. Caruso, A. Del Nevo, Electromagnetic coupling phenomena in co-axial rectangular channels, Fusion Eng. Des. 160 (2020) 111854.

[22] M.J. Bluck, M.J. Wolfendale, An analytical solution to electromagnetically coupled duct flow in MHD, J. Fluid Mech. 771 (2015) 595–623.

[23] C. Mistrangelo, L. Bühler, C. Koehly, I. Ricapito, Magnetohydrodynamic velocity and pressure drop in manifolds of a WCLL TBM, Nucl. Fusion 61 (9) (2021) 096037.

[24] L. Bühler, C. Mistrangelo, A simple MHD model for coupling poloidal manifolds to breeder units in liquid metal blankets, Fusion Eng. Des. 191 (2023) 113552.

[25] M. Tillack, Magnetohydrodynamic flow in rectangular ducts. Design equations for pressure drop and flow quantity, UCLA-Rep. UCLA-FNT 41 (1990).

[26] I.E. Idel'chik, in: D. Grunaer, P.E., IPST Staff (Eds.), Handbook of hydraulic resistance - Coefficients of local resistance and of friction, Israel program for scientific translations, Jerusalem, 1966.

[27] C. Fletcher, R. Schultz, RELAP5/MOD3 Code Manual, Tech. Rep., Nuclear Regulatory Commission, Washington, DC (United States). Div. of . . . , 1992.

[28] T. Rhodes, S. Smolentsev, Pressure drop in a prototypical 3D magnetohydrodynamic flow across contraction of a fusion blanket manifold, J. Nucl. Sci. Technol. 58 (8) (2021) 908–917.

[29] C. Mistrangelo, L. Bühler, V. Klüber, C. Koehly, Towards the simulation of MHD flow in an entire WCLL TBM mock-up, Fusion Eng. Des. 193 (2023) 113752.